Master's Thesis

Numerical and Theoretical Studies of Radiation from Plasma Dipole and its Applications

Salizhan Kylychbekov

Department of Physics

Graduate School of UNIST

2020

Numerical and Theoretical Studies of Radiation from Plasma Dipole and its Applications

Salizhan Kylychbekov

Department of Physics

Graduate School of UNIST

Numerical Study of Radiation from Plasma Dipole and its Applications

A thesis/dissertation
submitted to the Graduate School of UNIST
in partial fulfillment of the
requirements for the degree of
Master of Science

Salizhan Kylychbekov

14. 01. 2020
Approved by

_____

Advisor
Min Sup Hur

Numerical Study of Radiation from Plasma Dipole and its Applications

Salizhan Kylychbekov

This certifies that the thesis/dissertation of Salizhan Kylychbekov
is approved.

14.01.2020

signature

_____

Advisor: Min Sup Hur

signature

_____

Moses Chung

signature

_____

Eunmi Choi

Abstract

Localized plasma dipole oscillation technique was first proposed by Kwon K. et al in 2016 as an efficient terahertz radiation source [1]. This can be achieved by cross-shooting two-color ultrashort laser pulses into plasma and can be applied for diagnostic purposes as well. Ensemble of charged particles oscillating like plasma dipoles radiate EM waves at plasma frequency (ω_p) with narrowband spectrum and carry meaningful information about the bulk plasma. In particular, by measuring the frequency of radiated signals, local plasma density at the focused point can be detected. Comparing the new idea with the conventionally utilized techniques such as interferometry, reflectometry and Langmuir probes [2-4], we insist that our method has numerous advantages as a technique for measuring the density [5]. Theoretical estimations accompanied by 1D, 2D, and 3D PIC simulations indicated that embedded plasma dipole oscillators show complex behavior leading to harmonic generations and many nonlinear effects that require further investigation. In this thesis, THz radiation scheme and density reconstruction measurements are reported and the investigations about magnetic field effects and harmonic generations are introduced briefly.

Contents

List of Figures

List of Tables

Chapter 1 - Introduction

1.1 Plasma dipole oscillation (PDO) – novel idea

Dipole oscillations, being a fundamental concept in Electromagnetism textbooks, consist of opposite charge combinations accelerating in space. Radiation from dipole oscillations has been thoroughly studied by profound people. However, generating such a geometry in plasma has remained untouched in research community perhaps due to the complexity and availability. If the dipole oscillations can be generated and maintained at certain positions, the expected radiation guarantees many interesting applications.

Recently, it was reported by Kwon et al that it is possible to obtain a localized bunch of electrons oscillating in plasma and generating a coherent, narrowband radiation at plasma frequency. In this thesis, I will provide the summary of the extended research of radiation from that plasma dipole oscillations (PDO). In particular, terahertz radiation, density diagnostics, second harmonic generation, and diagnostics of magnetized plasmas will be reported.

Chapter 2 - Background Theory of Embedded PDO

2.1 Dipole radiation

Let us start from the very basics - electric dipoles so that everything would be neat and clear. Initially, one can assume two oppositely charged particles that are separated at a distance d apart as shown in figure 1.1.

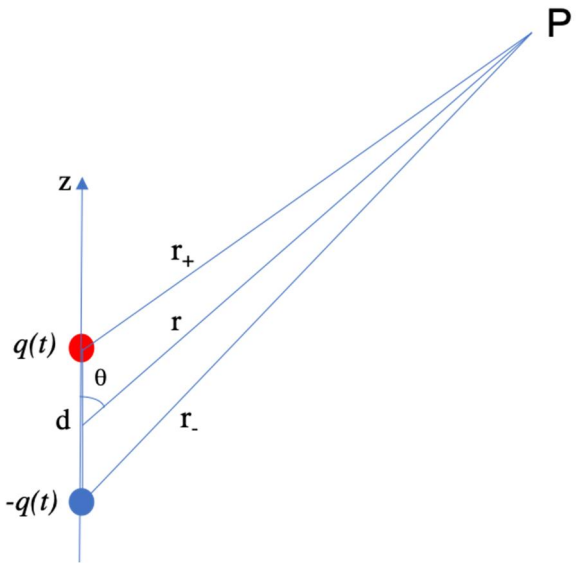

Figure 1.1 Electric dipole. Time dependence $q(t) = q_0\, cos(\omega t)$ and dipole moment, $p_0 \equiv q_0 d.$

Using the superposition principle, we can write the total Coulomb potential at the observation point P

$$V(\boldsymbol{r}) = \frac{1}{4\pi\epsilon_0}\left(\frac{q}{r_+} - \frac{q}{r_-}\right)$$

Note that the Binomial approximation will be particularly useful to round up the efficient part from Taylor expansion up to the first order,

$$\frac{1}{r_\pm} \cong \frac{1}{r}\left(1 \mp \frac{d}{r}\cos\theta\right)^{-\frac{1}{2}} \cong \frac{1}{r}\left(1 \pm \frac{d}{2r}\cos\theta\right)$$

$$\frac{1}{r_+} - \frac{1}{r_-} \cong \frac{d}{r^2}\cos\theta$$

The electric potential of the dipole at the first order can be computed using the approximation above,

$$V_{dip}(\boldsymbol{r}) = \frac{1}{4\pi\epsilon_0}\frac{\boldsymbol{p}\cdot\hat{\boldsymbol{r}}}{r^2}.$$

Now, we can introduce a time dependence the charges, $q(t) = q_0 \cos(\omega t)$, considering dipole moment

oscillates harmonically. The current is its time derivative,

$$\mathbf{I}(t) = \frac{dq}{dt}\hat{\mathbf{z}} = -q_0\omega\sin(\omega t)\,\hat{\mathbf{z}}$$

Dipole moment also is now dependent on time.

$$\mathbf{p}(t) = p_0\cos(\omega t)\,\hat{\mathbf{z}}, \text{ where } p_0 \equiv q_0 d$$

Time dependent vector and scalar potentials can be computed using the current and dipole moments,

$$V(\mathbf{r},t) = \frac{1}{4\pi\epsilon_0}\frac{1}{r}\int \rho(\mathbf{r}',t_r)d\tau' = \frac{1}{4\pi\epsilon_0}\frac{q}{r}$$

$$\mathbf{A}(\mathbf{r},t) = \frac{\mu_0}{4\pi}\int \frac{\mathbf{J}(\mathbf{r}',t_r)}{r}d\tau'$$

where $q = \int \rho(r',t_r)d\tau'$ and $t_r \equiv t - \frac{r}{c}$ is retarted time

Since it is now time-varying, we need to consider travel-time of the information using the retarted time concept:

$$V(\mathbf{r},t) = \frac{1}{4\pi\epsilon_0}\left\{\frac{q_0\cos[\omega(t-r_+/c)]}{r_+} - \frac{q_0\cos[\omega(t-r_-/c)]}{r_-}\right\}$$

$$\mathbf{A}(s,t) = \frac{\mu_0}{4\pi}\hat{\mathbf{z}}\int_{-d/2}^{d/2}\frac{I(t_r)}{r}dz$$

Approximation: $d \ll r$ for $r_\pm = \sqrt{r^2 \mp rd\cos\theta + (d/2)^2}$

$$\frac{1}{r_\pm} \cong \frac{1}{r}\left(1 \pm \frac{d}{2r}\cos\theta\right)$$

$$\cos[\omega(t-r_+/c)] \cong \cos\left[\omega(t-r/c) \pm \frac{\omega d}{2c}\cos\theta\right] = \cos[\omega(t-r/c)] \mp \frac{\omega d}{2c}\cos\theta\sin[\omega(t-r/c)]$$

$$V(r,\theta,t) = \frac{p_0\cos\theta}{4\pi\epsilon_0 r}\left\{-\frac{\omega}{c}\sin[\omega(t-r/c)] + \frac{1}{r}\cos[\omega(t-r/c\ )]\right\}$$

In the limit $r \gg 2\pi c/\omega = \lambda$, potential reduces to $V = \frac{p_0 \cos\theta}{4\pi\epsilon_0 r^2}$

$$V(r,\theta,t) = \frac{p_0\omega}{4\pi\epsilon_0 c}\left(\frac{\cos\theta}{r}\right)\sin[\omega(t-r/c)]$$

$$\mathbf{A}(s,t) = \frac{\mu_0}{4\pi}\hat{\mathbf{z}}\int_{-d/2}^{d/2}\frac{I(t_r)}{r}dz$$

$$\mathbf{I}(t) = \frac{dq}{dt}\hat{\mathbf{z}} = -q_0\omega\sin(\omega t)\,\hat{\mathbf{z}}$$

$$\mathbf{A}(r,t) = \frac{\mu_0}{4\pi}\int_{-d/2}^{d/2}\frac{-q_0\omega\sin[\omega(t-r/c)]\hat{\mathbf{z}}}{r}dz$$

$$\mathbf{A}(r,\theta,t) = -\frac{\mu_0 p_0\omega}{4\pi r}\sin[\omega(t-r/c)]\hat{\mathbf{z}}$$

Equipped with $V(r,\theta,t)$ and $\mathbf{A}(r,\theta,t)$, obtaining **E** and **B** just needs several steps from Maxwell's equations when

$$\mathbf{E} = -\boldsymbol{\nabla}V - \frac{\partial\mathbf{A}}{\partial \mathrm{t}}$$

$$\mathbf{B} = \boldsymbol{\nabla}\times\mathbf{A}$$

First, calculate $\boldsymbol{\nabla}V$

$$\boldsymbol{\nabla}V = \frac{\partial V}{\partial r}\hat{r} + \frac{1}{r}\frac{\partial V}{\partial\theta}\hat{\theta}$$

$$\boldsymbol{\nabla}V = -\frac{p_0\omega}{4\pi\epsilon_0 c}\left\{\cos\theta\left(-\frac{1}{r^2}\sin\left[\omega\left(t-\frac{r}{c}\right)\right]-\frac{\omega}{rc}\cos\left[\omega\left(t-\frac{r}{c}\right)\right]\right)\hat{r} - \frac{\sin\theta}{r^2}\sin\left[\omega\left(t-\frac{r}{c}\right)\right]\hat{\boldsymbol{\theta}}\right\}$$

$$\boldsymbol{\nabla}V \cong \frac{p_0\omega^2}{4\pi\epsilon_0 c^2}\left(\frac{\cos\theta}{r}\right)\cos\left[\omega\left(t-\frac{r}{c}\right)\right]\hat{\boldsymbol{r}}$$

$$\frac{\partial\mathbf{A}}{\partial t} = -\frac{\mu_0 p_0\omega^2}{4\pi r}\cos[\omega(t-r/c)](\cos\theta\,\hat{\boldsymbol{r}} - \sin\theta\,\hat{\boldsymbol{\theta}})$$

$$\boldsymbol{\nabla}\times\mathbf{A} = \frac{1}{r}\left[\frac{\partial(rA_\theta)}{\partial x} - \frac{\partial A_r}{\partial\theta}\right]\hat{\phi} = -\frac{\mu_0 p_0\omega}{4\pi r}\left\{\frac{\omega}{c}\sin\theta\cos[\omega\left(t-\frac{r}{c}\right)] + \frac{\sin\theta}{r}\sin[\omega(t-\frac{r}{c})]\right\}\hat{\boldsymbol{\phi}}$$

$$\boldsymbol{E} = -\boldsymbol{\nabla} V - \frac{\partial \mathbf{A}}{\partial t} = -\frac{\mu_0 p_0 \omega^2}{4\pi}\left(\frac{\sin\theta}{r}\right)\cos[\omega(t - r/c)]\hat{\boldsymbol{\theta}}$$

$$\boldsymbol{B} = \boldsymbol{\nabla} \times \mathbf{A} = -\frac{\mu_0 p_0 \omega^2}{4\pi c}\left(\frac{\sin\theta}{r}\right)\cos[\omega(t - r/c)]\hat{\boldsymbol{\phi}}$$

These fields are the radiated signals from the simple, oscillating electric dipole. Figure 1.2 shows the geometry of Electric and Magnetic fields of the emitted waves. Black plates represent two varying charge structures. As their value oscillate, EM waves will propagate from that source. In the remaining part of the thesis, large number of coherently oscillating plasma dipoles will be discussed, as an extension for the electric dipole radiation.

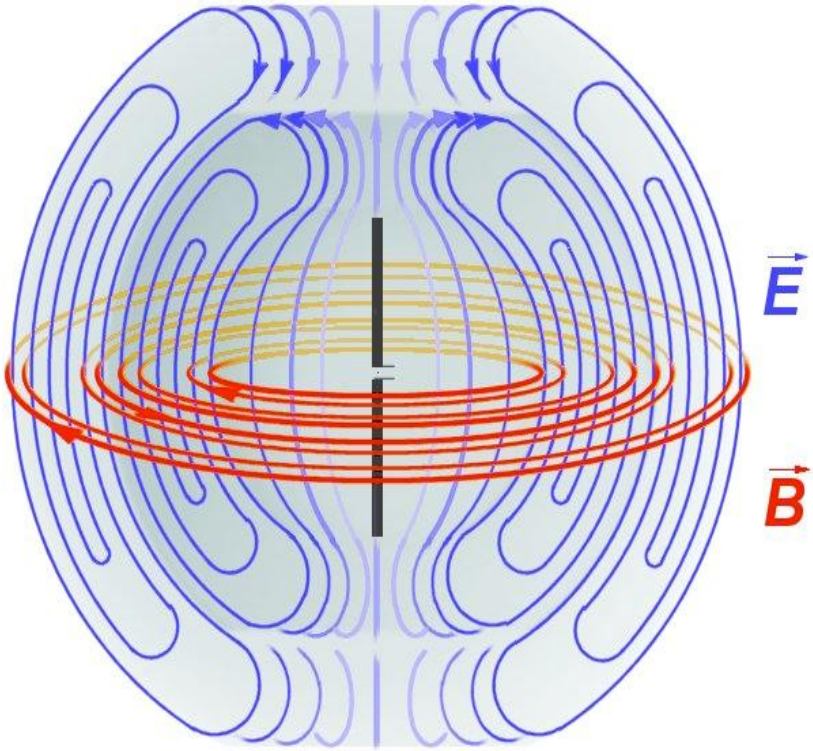

Figure 1.2 Radiation from the oscillating electric dipole. The upper and lower plates represent charges. E and B fields are transverse as found by analytical solution.

2.2 Mechanism - embedding plasma dipole oscillators (PDO) colliding detuned laser pulses

The idea of exciting PDOs by lasers was first proposed by Kwon K et al in 2016 [1] as a potential source of terahertz radiation, accomplished by shooting the counter-propagating ~30fs long pulses into

a preformed plasma. One should not get confused by thinking that PDOs exist as parts of Langmuir waves; they are different. Langmuir waves propagate in plasma if gets disturbed by ultra-intense laser pulses or beams of particles. In contrast, PDOs are independent and localized that oscillate around the prescribed position. They should be distinguished for the sake of clarity, and the obtaining method is described below.

Plasmas are well accepted as quasi-neutral. If we accomplish dragging the electrons by an electric force, it would create charge separation between the ions. Once released, the electrons will oscillate around the background ions at plasma frequency as shown in figure 2. Although the charge separation was reported in many articles, all of them were about plasma waves. Since one need a transient force to displace the electrons, lasers offered an ultimate choice. By slightly detuning the wavelengths of the laser pulses, a ponderomotive beat potential wave can be obtained:

$$\phi_{PM} = 2a_0^2 e^{-\left(\frac{(z/c-t)^2}{\tau^2}+\frac{(z/c+t)^2}{\tau^2}\right)} \cos\left((k_1+k_2)z-(\omega_1-\omega_2)t\right)$$

The wave moves with phase a velocity of $v = \frac{\omega_1-\omega_2}{k_1+k_2} \ll c$, and captures the bunches of electrons in its way forming a train of micro-bunches with longitudinal and transverse dimensions relevant to the spot radius and pulse width of the lasers pulses. Ions, on the other hand, are very heavy and slow compared to electrons, so that in the high frequency regime of electrons, they can be regarded as stationary. From this point, two regimes exist as candidates depending on the field strengths of the incident lasers.

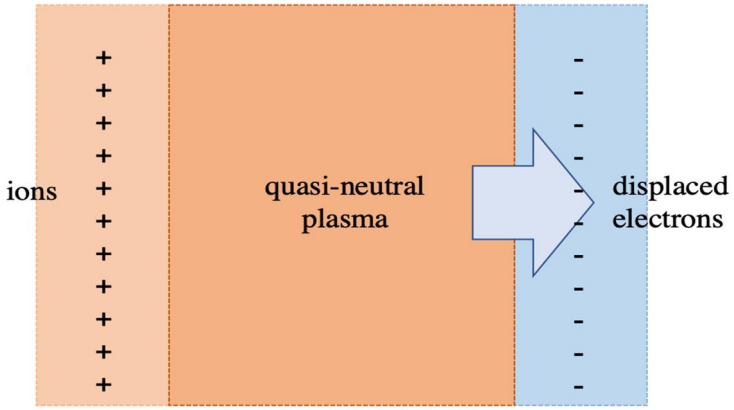

Figure 2.1 Plasma dipole formation in a quasi-neutral plasma.

2.2.1 Nonlinear current

This technique employs low-intensity lasers (for $a < 0.01$, where $a = {eE_0}/{mc\omega_0}$ is the normalized vector potential of the laser pulse). The purpose of using the lower intense pulses is to overcome the wave-breaking limit. In the region where the pulses overlap, the beat potential wave excites the plasma, and the response to that can be computed from fluid equations using linearization up to higher orders.

$$\delta n = \frac{1}{2}\hat{n}\left(e^{ik_1 x - i\omega_1 t} + e^{-ik_2 x - i\omega_2 t}\right) + c.c.$$

$$\delta v = \frac{1}{2}\hat{v}\left(e^{ik_1 x - i\omega_1 t} + e^{-ik_2 x - i\omega_2 t}\right) + c.c.$$

The current density can be then computed as

$$\delta J = -en_0\delta v - e\delta n\delta v$$

Only the direct current part of J remains in the steady state limit, where the oscillating part gets averaged out, and it fulfills the nonlinear component.

$$J_{dc} = -\frac{1}{2}e(\hat{n}\hat{v}^* + \hat{n}^*\hat{v})$$

J_{dc} is responsible for the dipole build-up as long as the pulse collision time is comparable to the dipole scales. I will keep it short here and further analysis can be found from M. Cho et al [] article.

2.2.2 Trapping the electrons

The same beat potential with $a > 0.1$ can cross the wavebreaking threshold, where particle trapping is enabled to obtain PDOs efficiently. The beat wave, moving in the region, captures electrons and drags them together as micro-bunches. Due to the charge separation, a restoring force for the electrons start to function and after the potential train leaves the region, micro-bunches phase mix gradually and start to oscillate in phase as a single bunch as shown in fig. 5b [1]. This oscillating plasma dipole generates radiation at plasma frequency, which is tunable by varying the density of background plasma. Optimization for the efficient generation is well discussed in using Force-balance model [1].

Chapter 3 – Radiation

3.1 Do plasma oscillations radiate?

Plasma oscillations are bit intricate when it comes to the radiation emission because they exist as part of the Langmuir waves, which are electrostatic and longitudinal. It is a well-known concept Langmuir waves do not emit radiation due to their dispersion relation, figure 6. No direct way of interaction is possible between the electromagnetic waves and Langmuir wave except at k = 0 mode. However, there were many good articles reporting different schemes for coupling the EM waves with Langmuir waves to enable the energy exchange between them [18].

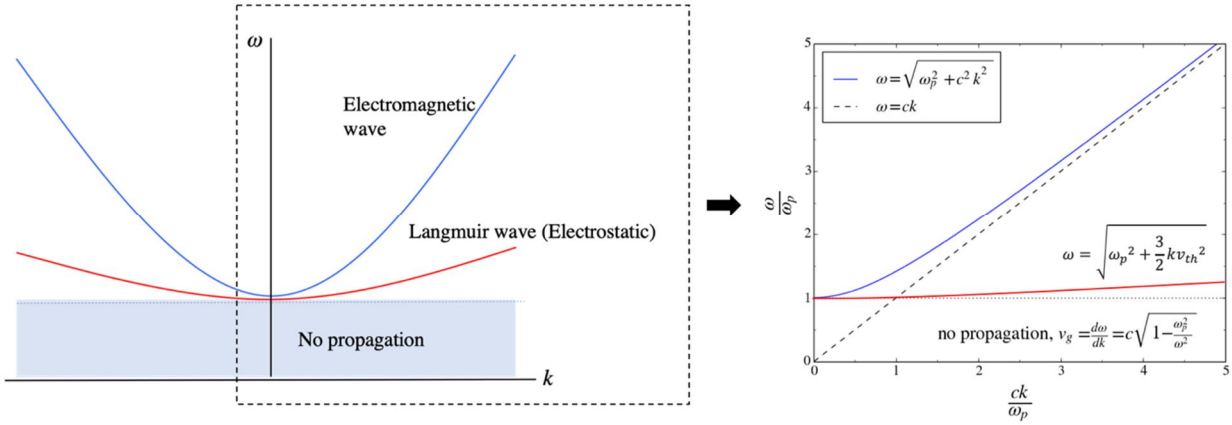

Figure 3.1 Dispersion relations of electrostatic and electromagnetic waves in an unmagnetized plasma. Right figure is derived from the left one. It shows that the only possible condition where the energy exchange can happen between the EM and electrostatic waves is at k=0. This implies that there does not exist direct way of converting the Langmuir wave to electromagnetic wave, unless additional mechanism is introduced, such as wave-wave coupling, Linear Mode Conversion, and etc.

Plasma dipole oscillations, in contrast, can be regarded an ensemble of charged particles forming local oscillations and emitting radiation as electric dipoles [11]. Linear mode conversion, nonlinear wave-wave interaction, quasi-mode conversion, and many reports were published about other ways of getting electromagnetic radiations from Langmuir waves by introducing intermediate couplings [17-19, 40]. By placing a steep density gradient, the mode exchanges can be enabled, or using density ripples one can obtain nonlinear currents that emit radiation. Many of them are wideband radiation. However, localized plasma dipoles radiate with narrowband frequency spectrum.

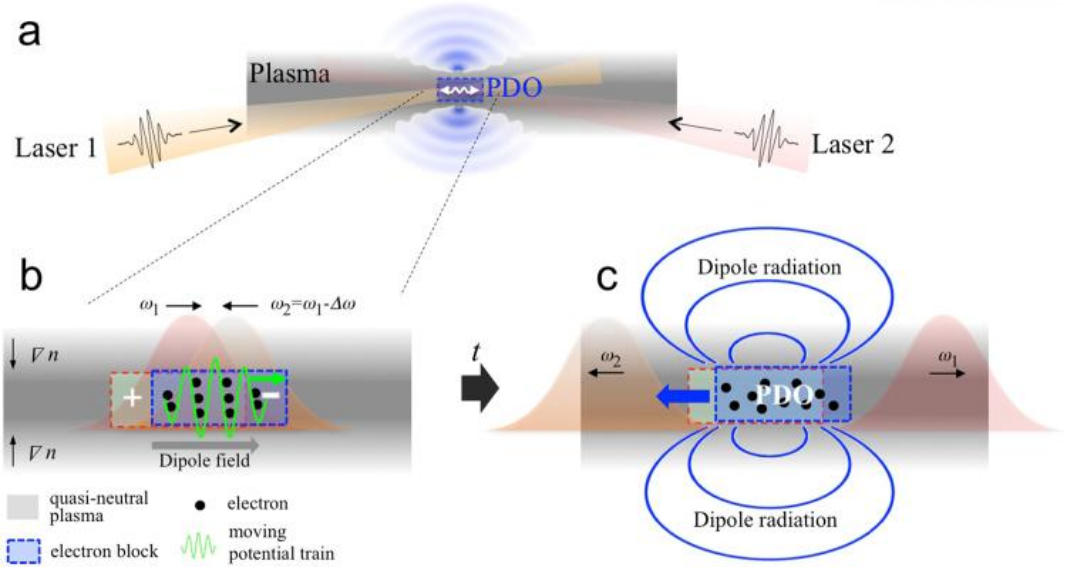

Figure 3.2 Obtaining a plasma dipole oscillation by trapping the electrons in a Ponderomotive beat wave. In the actual simulation, we used $\lambda 1 = 800nm, \lambda 2 = 779nm$. Pulse duration $\tau = 30fs$; Normalized laser field amplitude, $a_0 = \frac{eE_0}{mc\omega} = 0.3$ and plasma density, $\omega_p = \sqrt{\frac{n_0 e^2}{m\epsilon_0}}$, $n_0 = 4.96 \times 10^{18} cm^{-3}$.

3.2 PDO as a radiation source

Plasma dipoles oscillate at plasma frequency and radiate electromagnetic waves. The following figure is the result of proof-of-principle work done by simulation. The parameters of the simulation are given in the caption.

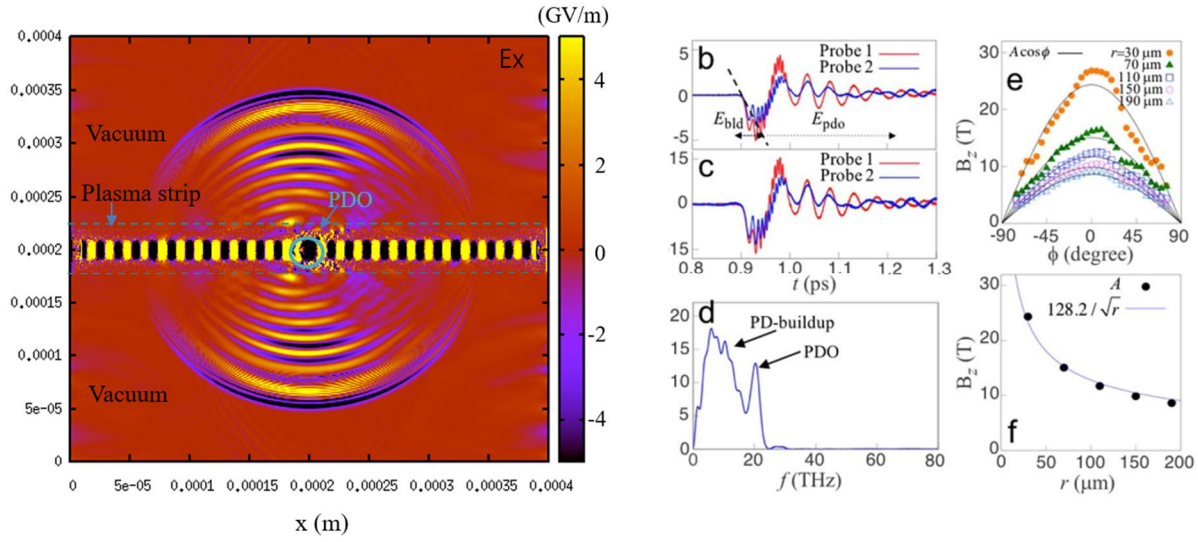

Figure 3.3 Radiation obtained from plasma dipole oscillations. 2D PIC simulation results were obtained. (a) Shows the configurations. Plasma is very narrowly put and of trapezoidal shape: 180μm-190 μm,

190 μm - 210 μm of n0 density, and 210 μm - 220 μm decreasing ramp. Wavelengths of the lasers: $\lambda_1 = 800nm, \lambda_2 = 780nm$. Pulse duration $\tau = 30$fs. Normalized laser field amplitude, $a_0 = \frac{eE_0}{mc\epsilon_0} = 0.3$; remaining simulation parameters are given in Part 4.2. (b),(c) Shows the readings of probes in the dipole center with 1 μm difference in y direction. It shows coherence of the ensemble oscillating as a single bunch. (d) Shows the Fast Fourier Transformed data of the electric field of the radiated signal. It has peaks at plasma frequency. The lower frequency, broadband part is probably from the dipole build-up site. (e-f) shows the propagation and angular coherence of the radiated signal. These features strongly imply that the radiation is from the localized plasma dipole oscillations.

Chapter 4 – New technique to measure local plasma density

Motivation

Plasma density is one of the most crucial parameters that gets involved in all characterizations, including the wave propagation inside the plasma, its permittivity, dielectric properties, and instabilities. Accurate assessment of it plays extreme importance. Although there have been numerous techniques of measuring the density, all of them are far from being a perfect candidate for local detection. In this chapter, we report the new technique that measures the plasma density by analyzing the spectra of radiated signals from PDOs. And also, simulation results, analysis, including pros and cons will be presented.

4.1 Method

One application of the radiation from PDOs is the measurement of local densities. Unlike conventional techniques such as interferometry, reflectometry and various scattering options, it detects the density at distinct points up to the dimensional precision comparable to the dipole size. In short, the measurement method comprises three steps:

1. Focusing the laser pulses to the desired position at plasma
2. Detecting the radiation from the generated plasma dipole oscillations
3. Fast Fourier transform the signal into frequency domain to check the frequency components

Since the plasma radiates dominantly at plasma frequency ($\omega_p = \sqrt{\frac{ne^2}{m\varepsilon_0}}$), it is possible to get an information about the background plasma density from $\omega_p \propto \sqrt{n}$, see fig. 7d.

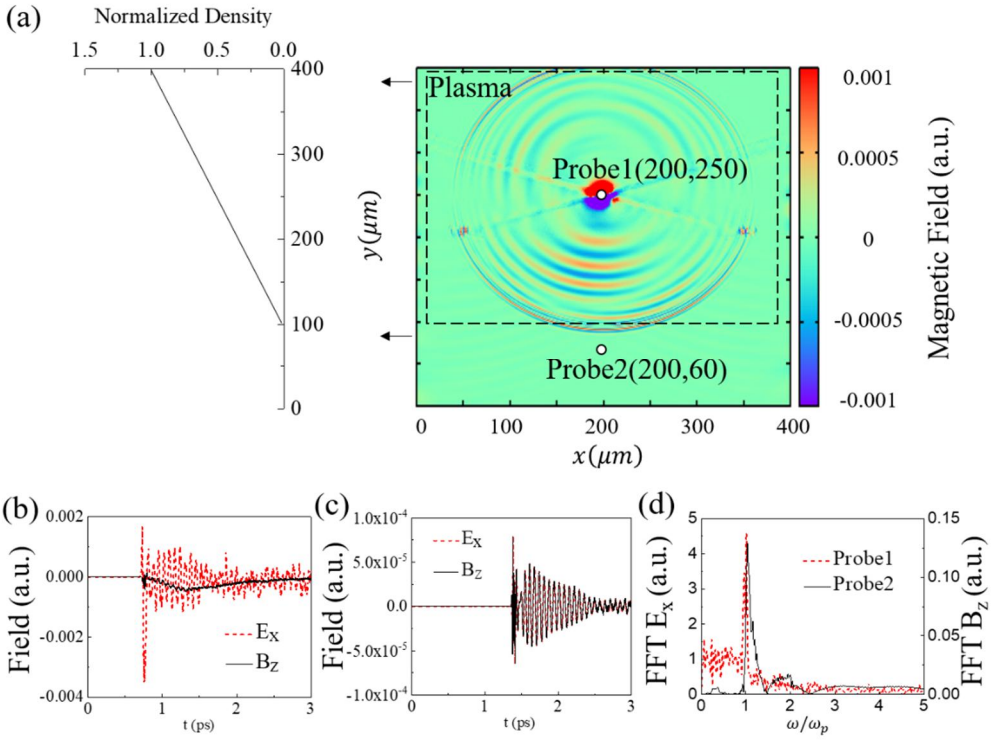

Figure 4.1 2D PIC simulation of radiation emitted from plasma dipole osicllations. (a) Simulation domain of 400μm by 400μm size and plasma is inside the dahsed line strip. (b) Shows two signals of Ex vs t and Bz vs time at the center of the dipole. (c) Shows Ex vs t and Bz vs t signals in vacuum. These signals are radiated from the dipole. (c) Fast Fourier Transforms of Ex signals. Red dashed line - from Probe 1 at the dipole center. Black line is from Probe 2 in vacuum. The peaks at ω_p match and the dipole emits radiation at plasma frequency.

Fig. 7 was obtained from the 2D PIC simulation. Dipole is created by two obliquely propagating pulses with wavelengths of 780nm and 800nm. The normalized laser amplitude is in the range of

$a_0 \sim 0.3$; starting from $a_0 > 0.5$ lasers can be regarded as relativistic. As mentioned earlier, if the amplitude is set to be smaller, then non-linear current mechanism will be important for dipole generation, rather than electron trapping in the potential beat wave. Oblique collision was employed to increase the efficiency of radiation, and also to get a better resolution. Oblique incidence also enhances the utility by disabling the need for the movement of launching positions. From figure 8, one can see the counter-propagating scheme to measure the density, where the lasers are set to be movable, which is unlikely feasible in real life experiments, or at least overcomplicates the construction of the observation system.

4.2 Results

The simulation was done by PIC code. The mesh size dimensions used such as $\Delta x = 0.05\mu m$ and $\Delta y = 0.2\mu m,$ respectively. This resolves the laser wavelength approximately by 20 and 5. The resolution in x-direction is higher because laser propagates in that direction. In addition, anisotropy in mesh size helps to avoid numerical dispersion. The time step $\Delta t = 1.6 \times 10^{-16}$s was used; this obeys the CFL condition. N=10/cell was used. The domain of the simulation was set, $x = 400\mu m$ by $y = 400\mu m$. As dipole starts its functioning, it starts to radiate at ω_p, see fig. 7a. Two probes were placed artificially to check the electric and magnetic signals at the desired positions. Probe 1 at the dipole center and Probe 2 in vacuum position. Lasers got launched from two sides at $(x, y) = (0\mu m, 340\mu m)$ and $(x, y) = (400\mu m, 340\mu m)$. They collide at $y = 250\mu m$. Fig. 7c shows Ex and Bz values at probe 1 that construct non-zero curl, which are the reasons for the radiation. Laser pulses overlap at $t \approx 7.31$s and Ex, Bz – t fits to this fact. The radiated signal was observed at probe 2 is shown in fig. 7d. The frequency components of the signals from the center and vacuum match. This is the key idea to make use of to measure the density at that dipole location.

The next step is reconstructing density profile by measuring different points. Fig. 8 shows the primitive idea consisting of the 3 step work. In fig. 8b the emitted signals are shown as Bz vs time and their Fast Fourier transformed picture. The domain was set to have linearly increasing density along y, but homogeneous along x-direction. The frequency spectra confirm this well, fig. 8b. Finally, fig. 8c provides the final step of reconstructing the density profile.

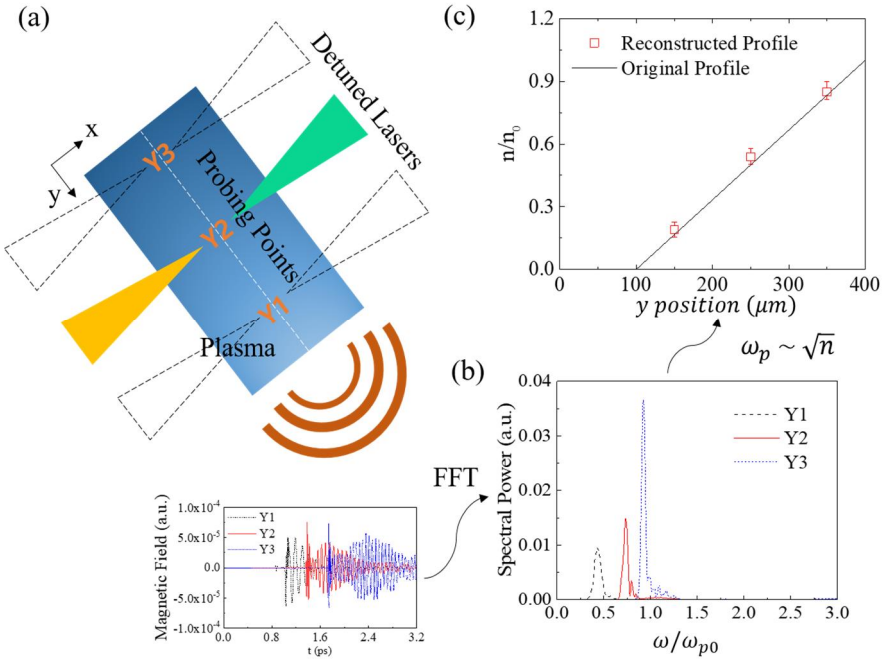

Figure 4.2 Measuring plasma density using radiation spectra involves three steps. (a) Counterpropagating and detuned pulses should be focused at the desired point. Magnetic field vs. time of probe readings (lower graph) at $Y_{1,2,3} = 150\ \mu m, 250\ \mu m, 350\ \mu m$. (b) Power spectra of the data in frequency domain obtained from FFT. Frequency is normalized by the plasma frequency of n_0. (c) Density reconstruction. Vertical axis indicates density normalized by $n_0 = 4.96 \times 10^{18}\ cm^{-3}$; horizontal axis is the direction of the density gradient (y direction of the simulation domain). The error bars originate from the spectral full bandwidth of the radiation at the half-maximum (FWHM).

In reality, however, the conditions are harsher than we have assumed. Changing the laser launching and nozzles for the detection are not easily available. One way of overcoming this challenge is using the oblique or pulses launched at angles. Fig. 9 demonstrates the simulations which confirm the validity of our assumption. It was discussed in Chapter 3 as well that obliquely collided lasers have complex overlapping regions which enhances the efficiency of the radiation generation accordingly. Although preliminary effort was done for this purpose, the efficiency should be thoroughly studied in the future.

4.2.1 Linearly density profiles

Linearly increasing density profiles are the simplest and should be investigated by the first chance. Fig. 8c shows 3 different density slopes and dots are the measured points. All of the simulation parameters are same; the only difference is in plasma density distribution over the simulation domain. The measured points show well correspondence with the original profile data.

In addition, angular dependence was also briefly summarized in fig. 8. 3 angle sets were utilized for the laser launching. 30°, 15°, and 0°. As can be seen from fig. 8a, threshold angle can be set as 15° for which the dipole shows narrowband and reliable data, otherwise the radiated emitted has unreliable features.

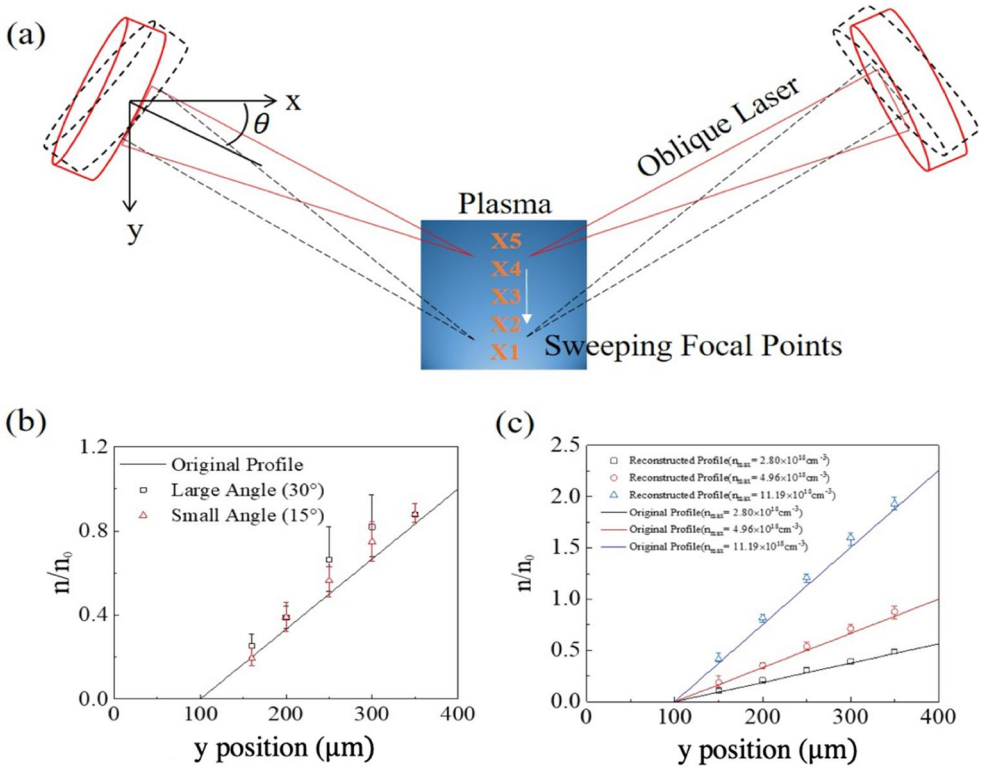

Figure 4.3 Obliquely propagating laser pulses and demonstrative density measurements (a) Schematic diagram of obliquely propagating lasers to induce the radiation. (b) Reconstructed density profile for small (15°) and large (30°) collision angles and (c) density reconstruction of three different gradients by sweeping shot angles of the pulses at fixed launching positions located far from the plasma. n_{max} in the legend represents the maximum density at $y = 400\ \mu m$. Vertical axes in (b) and (c) represent the density normalized by $n_0 = 4.96 \times 10^{18}\ cm^{-3}$; horizontal axes are the y-position along the gradient. Laser wavelengths are $\lambda_1 = 800$ nm, $\lambda_2 = 780$ nm and normalized peak amplitude $a_0 = 0.3$.

4.2.2 Nonlinear density profiles

For the sake of generality, the measurements for nonlinearly increasing density profiles were also conducted. In Cosine and exponentially increasing profiles are depicted in fig. 9. As the slope of the

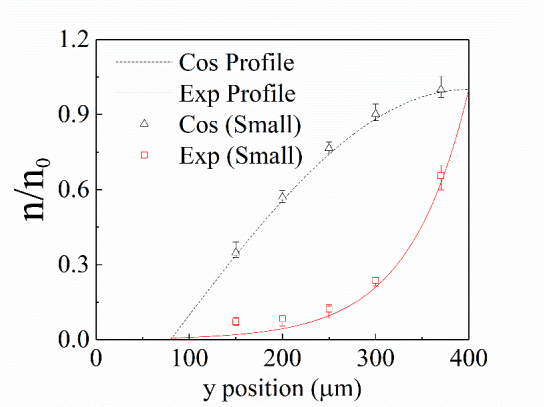

Figure 4.4 Reconstruction of the nonlinear density profiles, one is cosine (dotted, triangles) and the other is exponential (solid, rectangles). The exact profiles are $n/n_0 = cos[\pi(y-400)/640]$, and $n/n_0 = exp[(y-400)/100]$. The laser pulses made small angle collisions (i.e. under 15°). $n_0 = 4.96 \times 10^{18}\ cm^{-3}$ and the laser parameters are the same as in Fig. 4.3

density gradient gets steeper, so the radiation starts to get broader giving a hard time to recognize the plasma frequency. For this purpose, we conducted further research to verify our doubts. Indeed, when the density had extreme slopes of changes, the dipole fails to oscillate homogeneously, thus fails to sustain reliable data about the local density with broad peak spectrum making us hard to distinguish the main peak.

4.2.3 Limitations

This method has one major disadvantage. The emitted signal is radiated at plasma frequency, which simply gets cut-off from the ambient plasma if there is any density bump. To demonstrate this, we present fig. 10. We reconstruct the density profile over 200μm to 300μm, where the trough I located. As shown in fig. 10a, reconstructed dots misrepresent the data. In the unpresented data, we found that the main radiation is absorbed by the plasma, so the signal is very weak where the troughs exist. One can spot that measured points starting from y=200μm to 300μm lead to the correct measurements and signals were also strong and narrowband (not presented here). Thus, troughs absorb the waves emitted from less dense regions, so it is called in plasma physics as waves were cut-off.

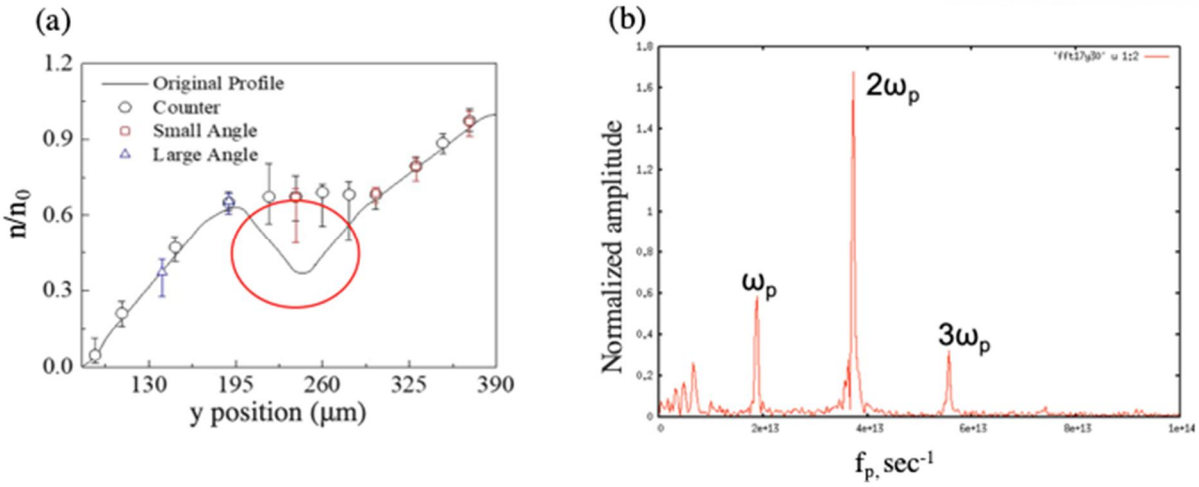

Figure 4.5 Reconstruction of the non-monotonically-increasing density profiles. Vertical axis: reconstructed value normalized by the maximum value $n_0 = 4.96 \times 10^{18}\ cm^{-3}$. The normalized peak amplitude of the laser field is $a_0 = 0.3$. The simulation domain has the same dimension as in Fig. 4.3 and Fig. 4.4 The wavelengths of the laser pulses are 800 nm and 780 nm, the pulse duration is 30 fs and spot size is $5\ \mu m$. (b) As laser intensity gets higher to relativistic regime, harmonic emission gets enabled. This can overcome the bump issue. This is a new topic for study.

Chapter 5 – Conclusion

5.1 Higher harmonic radiation

Density measurements can be enhanced further. First, it is worth to note that when the laser field amplitude reaches the relativistic limit, the harmonic series, especially the second harmonic dominates the frequency spectrum of the radiation. Since the second harmonic has much higher frequency than that of the fundamental, it is expected to pass through the density bumps for which the fundamental harmonic waves fail to do so.

5.2 Magnetic field effects

Next interesting moment is the magnetic field inclusion. In nature, magnetic field exists everywhere. It is worth to study the dipole formation and the effect that radiation will get as we turn on the magnetic field effects. Of course by the dispersion relation we will expect the inclusion of transverse motion of the electrons along with longitudinal oscillations. Its rotational motion at cyclotron frequency will also emit radiation, but in which regime and how they will enhance or affect the duration of the dipole are still unanswered yet.

5.3 Thermal effects

Thermal effects on plasma were already studied. In fig. 11, it is possible to spot the temperature of the plasma and its impact on the oscillation of electrons. Thermal energy is nothing but the average kinetic energy of the constituting particles. If it is high, then it would enhance the random motion, which diminishes the harmonic motion of electron ensemble as a dipole. Thus, thermal effects should adversely affect the system. Interestingly, we saw that the thermal contributions to the instability of the dipole is negligible as long as a_0 – normalized laser peak is high enough

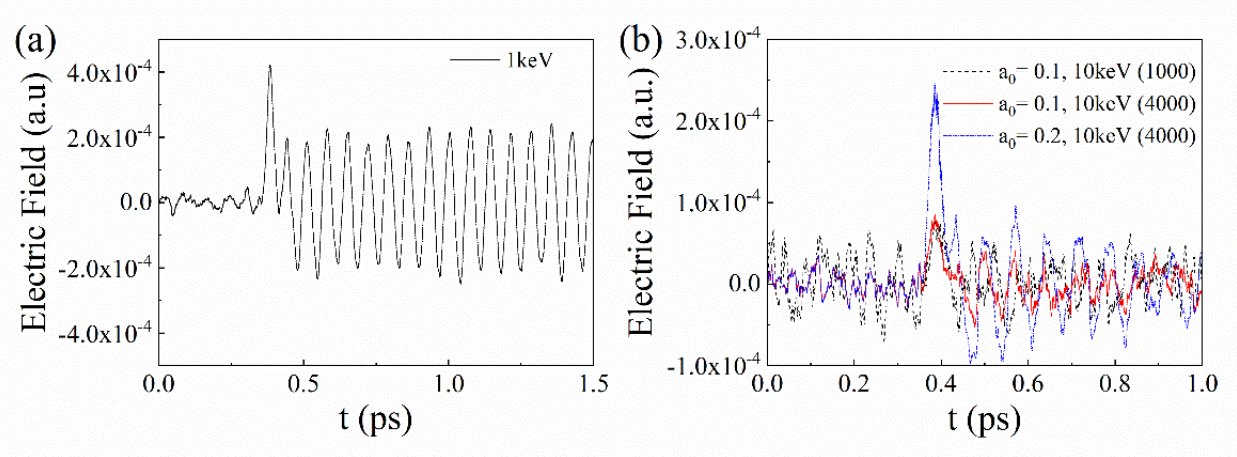

Figure 5.1 Generation of the dipole oscillation in thermal plasmas with (a) $T_e = 1\ keV$ and (b) 10 keV. The normalized amplitude of the driving laser pulses is $a_0 = 0.1$ for 1 keV and $a_0 = 0.1$ and 0.2 for 10 keV. The simulations were repeated increasing the number of simulation particles per cell, n_s, to reach the quasi-saturation of the numerical noise. In (b), n_s is denoted in the parentheses of the legend. The numerical-thermal noise decreases significantly for the larger n_s.

5.4 Applications for real systems

We have studied 2D PIC simulations in settings relevant to laser-plasma interactions system, where the plasma density is in scales of 10^{18} cm^{-3}, and the driving wavelength is ~1μm. These parameters can be tuned for the use in diagnostics of other systems, e.g., fusion plasmas.

Table 5.1 Parameters that we used for studies. They are relevant for laser-plasma interactions field. These parameters can be tuned for other systems. Preparations are going on to apply the dipole concept to low intense, low density plasma case.

Parameter	Lower	Upper
n_e	5 x 10^{20} m^{-3}	0.5 x 10^{25} m^{-3}
T	1 eV	1 keV
a_0	0.0005	0.7
λ	600nm	1000nm

5.5 Collisional effects

Our method depends on the collisions between the electrons and neutrals or electrons and ions because they can disrupt the long duration, coherent oscillation. The similar issue is expected to arise in other cross-beam schemes (designed for other purposes than diagnostics) such as the plasma photonic crystal [36] or plasma holography [37]. Unlike in fully ionized plasmas, in low density plasmas, the collision between the electron and neutrals is non-negligible. The collision frequency for electron-neutral can be estimated by $\nu_{en}[\mathrm{s}^{-1}] \sim 2\times10^{-7} n_n[\mathrm{cm}^{-3}](T_e[\mathrm{eV}])^{1/2}$ [38], however, is much lower than the plasma frequency ($f_p = \omega_p/c$); for low temperature plasmas, which can be obtained from breakdown of gases with a few Pascals of pressure, $n_n \sim 10^{13}$ cm^{-3} and $T_e \sim 1$ eV, leading to $\nu_{en} \sim$ 1 MHz, while the plasma frequency is in the range of a few GHz for $n_e \sim 10^{12}$ cm^{-3}. In Tokamaks, in particular, in the edge parts, the temperature is of order 1 keV, but the density is very low, so the collisional frequency remains to be much lower than the plasma frequency; not only in the edge, but even near the divertor, where the neutral density is much higher, $n_n < 10^{14}$ cm^{-3}, the ν_{en} is lower than the plasma frequency $f_p \sim$ 1 GHz, and not enough to affect significantly. Thus, the electron-neutral collisions are argued to be not enough to critically affect the PDO emission in most of the plasma sources.

The electron-ion collisions, on the other hand, in high-density, laser-produced plasmas can disrupt the PDO oscillation. Again, from the electron-ion collision frequency given by ν_{ei} [s^{-1}] $\simeq 3\times10^{-5} n_e$ [cm^{-3}]$(T_e[\mathrm{eV}])^{-3/2}$ [38], for $n_e \sim 10^{18}$ cm^{-3} which is used throughout this thesis, T_e should be larger than 10 eV to keep ν_{ei} below 10 percent of f_p. The condition $T_e > 10$ eV is the case for many laser-plasma interactions. Furthermore, the electron bunch of the plasma dipole is thermal since the dipole is generated from the electron trapping, and it is prone to stochastic heating. From Ref. [1], it is observed that the dipole bunch has the thermal velocity in the order of $\beta = v/c$~0.01, which corresponds to $T_e \sim 50$ eV, and is high enough that the electron-ion collision effect, ν_{ei} is negligible. We should note that the PIC code does not include the collisional phenomena, so the results are selective, however, still highly argued as valid since the electron-ion collision, as was seen above, is negligible in high temperature.

5.6 Propagation of the emitted wave

Another question is the propagation of the emitted wave from plasma dipoles. The intensity decay of the radiated wave over distance is pertinent to the issue of detector's sensitivity. In Ref. [1], it was demonstrated that the emission from the PDO obeys the pattern of the two dimensional dipole radiation. In addition, we did similar analysis (not published) that showed the decay of the field strength over the propagation distance. In the three dimensions, the field strength of the dipole radiation can be estimated by

$$E \sim E_0 \frac{\sigma_{di}}{r},$$

where σ_{di} is the width of the dipole and E_0 is the electric field value at the dipole, i.e. at $r \sim \sigma_{di}$. Note that the transverse size σ_{di} is approximately the same as the spot size σ of the laser pulse. Usually, σ is comparable to the plasma wavelength $\lambda_p = 2\pi c/\omega_p$. When the emitted field is measured at $r \sim N\lambda_p$, then $E \sim E_0/N$. In the laser-produced plasmas used throughout this paper, $N \sim 100$ and $E_0 \sim 1$ GV/m, leading to $E \sim 10$ MV/m at the observation point, which can be detected since it is strong enough. We take the similar estimation for the nuclear fusion or low temperature plasmas as well, $\lambda_p \sim 1$ mm $(n_e \sim 10^{14}$ cm$^{-3})$ and $N \sim 1000$ for the detection at 1 m apart. Noting that as $E_0 \propto n_e$, $E_0 \sim 10^5$ V/m and then the field measured at 1 m apart from the dipole will be of order a few hundred of V/m, and implying to be very strong and measurable.

5.7 Dipole formation – density steepness limitations and broadening of the spectrum

If the plasma density varies very sharply, the plasma dipole can not be formed coherently. This can be spotted by the broadening as the slope of the density gradient gets too high.

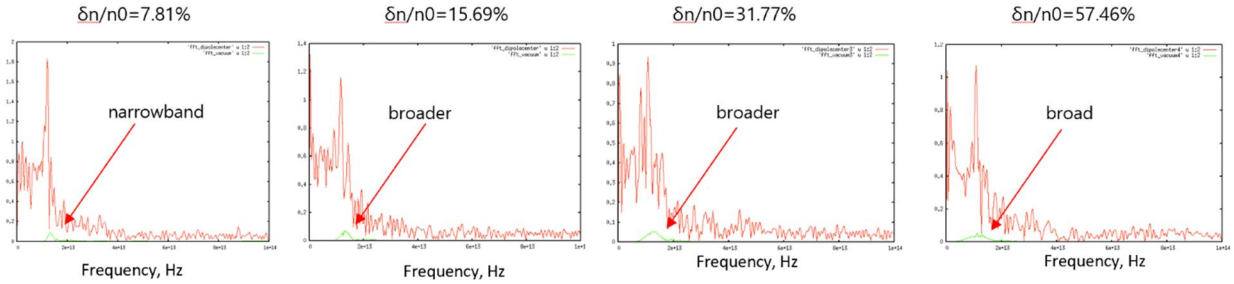

Figure 5.2 Broadening of the spectra due to the extre variation of the density along the transverse width of the dipole. The guaranteed region of the proper dipole oscillation is up to $\frac{\delta n}{n_0} = 15\%$; If along the dipole width the density varies too much, the dipole can not be formed properly and thus narrowband emission will not occur.

Conclusion

In this thesis, Plasma Dipole Oscillation concept was summarized. Its excitation in uniform, cold, unmagnetized plasma by detuned lasers was introduced. Then, we questioned whether it is possible to get radiation from the PDO or not. We moved to the main part of this thesis by presenting a new diagnostic technique to measure the local plasma density using the emitted radiation from PDOs. This technique is unique to pinpoint the plasma density at specific position. The precision and reliability of the dipole remains high unless the background plasma is extremely inhomogeneous, thermal[]. The dipole generation in magnetized plasmas and second harmonic generation is a future job.

Acknowledgement

It was a good moment to fulfill the Master's program at CPL under the supervision of professor M. Hur. I want to thank him as he supported us always and treated his students with special care and fatherly love. In addition, I also want to express my gratitude to Dr. T. Kang, Hyungseon, KyuBeen, Ookjoo, and Wonjun. They have been excellent, friendly, and supportive colleagues. Especially, we had so much fruitful scientific discussions with Dr. T. Kang. Finally, I want to thank the faculty members and Korean government for providing a scholarship and fund to do the fundamental science. With full credit, I can say that I owe them much. I wish this group and everyone all the best.

This research was supported the National Research Foundation of Korea (grant number NRF-2016R1A5A1013277), (grant number 2: NRF-2017M1A7A1A03072766), and other international collaborators.

References

[1] Kwon K B, Kang T Y, Song H S, Kim Y K, Ersfeld B, Jaroszynski D A and Hur M S 2018 High-Energy, Short-Duration Bursts of Coherent Terahertz Radiation from an Embedded Plasma Dipole *Sci. Rep.* **8**, 145

[2] Cherrington B E 1982 The use of Langmuir probes for plasma diagnostics: A review *Plasma Chemistry and Plasma Processing* **2**, 113–140

[3] Laviron C, Donné A J H, Manso M E and Sanchez J 1996 Reflectometry techniques for density profile measurements on fusion plasmas *Plasma Phys. Control. Fusion* **38-7**, 905-936

[4] Nagornyi D A, Nagornyi A G and Voznyi V I 2005 A microwave interferometer for steady-state plasma density measurements *Instrum. Exp. Tech.* **48**, 225

[5] Park H K 2019 Newly uncovered physics of MHD instabilities using 2-D electron cyclotron emission imaging system in toroidal plasmas Adv. Phys.:X **4**, 1633956

[6] A. J. H. Donné, C. J. Barth and H. Weisen 2008 Chapter 4: Laser-Aided Plasma Diagnostics *Fusion Science and Technology* **53:2**, 397-430, DOI: 10.13182/FST08-A1676

[7] Tokuzawa T *et al* 2018 Microwave frequency comb Doppler reflectometer applying fast digital data acquisition system in LHD *Rev. Sci. Instrum.* **89**, 10H118

[8] Mazzucato E 2014 Plasma Reflectometry *Electromagnetic Waves for Thermonuclear Fusion Research*, 123-162 doi.org/10.1142/9789814571814_0007

[9] Morales R B, Hacquin S, Heuraux S and Sabot R 2017 New density profile reconstruction methods in X-mode reflectometry *Rev. Sci. Instrum.* **88**, 043503 doi.org/10.1063/1.4979513

[10] Kang T, Kwon K B, Cho M H, Kim Y K, Hur M S, Park H K, Lee W 2018 Envelope-PIC Hybrid Method for the Simulation of Microwave Reflectometry *IEEE Trans. Plasma Sci*. **46**, 577

[11] Kylychbekov S *et al* 2020 Reconstruction of plasma density profiles by measuring spectra of radiation emitted from oscillating plasma dipoles *Plasma Sources Sci. Tech.* **(accepted)**

[12] Quevedo H J, McCormick M, Wisher M, Bengtson R D, and Ditmire T 2016 Simultaneous streak and frame interferometry for electron density measurements of laser produced plasmas *Rev. Sci. Instrum.* **87**, 013107 doi.org/10.1063/1.4940235

[13] David D R *et al* 1994 Measurement of Laser-Plasma Electron Density with a Soft X-ray Laser Deflectometer *Science* **265**, 514-517

[14] Vieux G, Ersfeld B, Farmer J P, Hur M S, Issac R C and Jaroszynski D A 2013 Plasma density measurements using chirped pulse broad-band Raman amplification *Appl. Phys. Lett.* **103**, 121106 doi.org/10.1063/1.4821581

[15] Li W M *et al* 2019 Bench test of phase measurement on dispersion interferometer for EAST *Rev. Sci. Instrum.* **90**, 026105 https://doi.org/10.1063/1.5058705

[16] Torrisi G et al 2016 Microwave frequency sweep interferometer for plasma density measurements in ECR ion sources: Design and preliminary results *Rev. Sci. Instrum.* **87**, 02B909 https://doi.org/10.1063/1.4933025

[17] Sheng Z M, Mima K, Zhang J, and Sanuki H 2005 Emission of Electromagnetic Pulses form Laser Wakefields through Linear Mode Conversion *Phys. Rev. Lett.* **94**, 095003

[18] Malaspina D M, Cairns I H, and Ergun R E The 2fp radiation from localized Langmuir waves 2010 *The Journal of Geophysical Research, Space Physics,* **145**

[19] Graham D B and Cairns I H 2015 The Langmuir waves associated with the 1 December 2013 type II burst, *Journal of Geophysical Research: Space Physics*, **120**, 6, 4126-4141

[20] Langmuir I, Compton K T 1931 Electrical discharges in gases part II. Fundamental phenomena in electrical discharges *Rev. Mod. Phys.* **3**,191

[21] Equipe TFR 1978 Tokamak plasma diagnostics *Nuclear Fusion **18***, 647

[22] Chen F F 2003 Langmuir Probe Diagnostics EE, UCLA; *Mini-Course on Plasma Diagnostics IEEE-ICOPS meeting, Korea*

[23] Ussenov Y A, E. Wahl V, Marvi Z, Ramazanov T S and Kersten H 2019 Langmuir probe measurements in nanodust containing argon-acetylene plasmas. *Vacuum* **166**, 15-25

[24] Siegfried H G and Redmer R 2009 X-ray Thomson scattering in high energy density plasmas *Rev. Mod. Phys*. **81**, 1625

[25] Kozlowski P M, Crowley B J B, Gericke D O, Regan S P & Gregori G 2016 Theory of Thomson scattering in inhomogeneous media *Sci. Rep.* **6**, 24283

[26] Segre S E 1999 A review of plasma polarimetry - theory and methods *Plasma Phys. Control. Fusion* **41**, R57

[27] Song H S, Cho M H, Kim Y K, Kang T Y, Suk H and Hur M S 2016 Measurement of local density and magnetic field of a magnetized plasma using Raman scattering from a focused laser pulse *Plasma Phys. Control. Fusion* **58**, 025006 doi.org/10.1088/0741-3335/58/2/025006

[28] Cho M H, Kim Y K and Hur M S 2014 Measuring the magnetic field of a magnetized plasma using Raman scattering *Appl. Phys. Lett.* **104**, 141107

[29] Jang H, Hur M S, Lee J M, Cho M H, Namkung W and Suk H 2008 A method to measure the electron temperature and density of a laser-produced plasma by Raman scattering *Appl. Phys. Lett.* **93**, 071506 doi.org/10.1063/1.2973395

[30] Ciocarlan, C *et al* 2013 The role of the gas/plasma plume and self-focusing in a gas-filled capillary discharge waveguide for high-power laser-plasma applications *Phys. Plasmas* **20**, 093108

[31] I. H. Hutchinson 2002 *Principles of Plasma Diagnostics* (Cambridge Univ. Press)

[32] Cho M H, Kim Y-K, Suk H, Ersfeld B, Jaroszynski D A and Hur M S 2015 Strong terahertz emission from electromagnetic diffusion near cutoff in plasma *New J. Phys.* **17**, 043045

[33] Hur M S and Suk H 2011 Numerical study of 1.1 GeV electron acceleration over a-few-millimeter-long plasma with a tapered density *Phys. Plasmas* **18**, 033102

[34] Yang X *et al* 2015 Chirped pulse Raman amplification in warm plasma towards controlling saturation *Sci. Rep.* **5**, 13333

[35] Vieux G *et al* 2017 An ultra-high gain and efficient amplifier based on Raman amplification in plasma *Sci. Rep.* **7**, 2399

[36] Lehmann G and Spatschek K H 2016 Transient Plasma Photonic Crystals for High-Power Lasers *Phys. Rev. Lett.* **116**, 225002

[37] Dodin I Y and Fisch N J 2002 Storing, Retrieving, and Processing Optical Information by Raman Backscattering in Plasmas *Phys. Rev. Lett.* **88**, 165001

[38] Sprangle P, Penano J R, Hafizi B, and Kapetanakos C A 2004 Ultrashort laser pulses and electromagnetic pulse generation in air and on dielectric surfaces *Phys. Rev. E* **69**, 066415 https://doi.org/10.1103/PhysRevE.69.066415

[39] Teubner U *et al* 1997 Observation of VUV radiation at wavelengths in the f_{p-} and $2f_{p-}$ wavelength range emitted from femtosecond laser-plasmas *Optics Communications* **144**, 217-221

[40] Timofeev I V, Annenkov V V, Volchok E P 2017 Generation of high-field narrowband terahertz radiation by counterpropagating plasma wakefields *Phys. Plasmas* **24**, 103106